Fusing GNSS, Dead-Reckoning, and Enhanced Maps for Road Vehicle Lane-Level Navigation

Rafael Toledo-Moreo, *Member, IEEE*, David Bétaille, *Member, IEEE*, François Peyret, and Jean Laneurit

***Abstract*—Nowadays, it is common that road vehicle navigation systems employ maps to represent the vehicle positions in a local reference. The most usual process to do that consists in the estimation of the vehicle positioning by fusing the Global Navigation Satellite System (GNSS) and some other aiding sensors data, and the subsequent projection of these values on the map by applying map-matching techniques. However, it is possible to benefit from map information also during the process of fusing data for positioning. This paper presents an algorithm for lane-level road vehicle navigation that integrates GNSS, dead-reckoning (odometry and gyro), and map data in the fusion process. Additionally, the proposed method brings some benefits for map-matching at lane level because, on the one hand, it allows the tracking of multiple hypothesis and on the other hand, it provides probability values of lane occupancy for each candidate segment. To do this, a new paradigm that describes lanes as piece-wise sets of clothoids was applied in the elaboration of an enhanced map (Emap). Experimental results in real complex scenarios with multiple lanes show the suitability of the proposed algorithm for the problem under consideration, presenting better results than some state-of-the-art methods of the literature.**

***Index Terms*—Enhanced maps, Global Navigation Satellite System (GNSS), maps, multisensor data fusion, navigation, particle filter.**

I. Introduction

In the frame of the European 6th framework program (e-SAFETY call) and particularly in the frame of the Cooperative Vehicle Infrastructure Systems (CVIS) integrated project, the researchers of the geolocalization division of the LCPC introduced the concept of enhanced map, or Emap [1]. Within CVIS, the POsitioning and MApping (POMA) subproject—to which LCPC belongs—aims at developing, testing and finally supplying applications with advanced positioning and mapping solutions. Some of these applications require lane-level accuracy, e.g., "Enhanced Driver Awareness" warning the driver of any hazard along its trajectory, or new services called "Lane Allocation" or "Intelligent Speed Alert." Emap, in combination with on-board vehicle sensors, have been introduced to make possible the determination of accurate lane occupancy and lane change when overtaking or splitting off to an exit for instance.

In this paper, we present the feasibility of a new Map Aided Localization (MAL) that extends the original concept to Emap (EMAL). With this concept, both ego-positioning of the vehicle and map-matching are achieved together in a unique process. Due to its accuracy and its completeness, the Emap offers *a priori* information of great interest with regard to the onboard sensors fusion algorithm, in the core of which it will be considered as a constraint. Additionally, a multiple hypotheses Emap tracking will be performed, using particle filter: here, this filtering strategy appears all the more interesting since the map itself contains many more alternatives than standard maps.

The rest of the paper is organized as follows. First, in Section II, some interesting works of the literature of this topic are analyzed. Section III summarizes the Emap contents and its creation process. The proposed data fusion algorithm that employs GPS/EGNOS, dead-reckoning, and Emap observations is explained in Section IV. Finally, the results achieved in our experiments and the conclusions obtained from them are discussed in Sections V and VI.

II. Related Work

In an urban environment, automotive applications cannot rely on GNSS based geolocalization only, since satellites outages are frequent, due to the surrounding building structures, tree canopies, and high vehicles [2]. Therefore, usual navigation generally couples dead-reckoning and GNSS positions or pseudo-ranges (distances to satellites), with a minimum of four satellites in the first case (loose coupling), whereas even one satellite brings about an observation that can update the navigation process in the second case (tight coupling). Usually in cars, dead-reckoning is based on the use of an onboard low-cost Inertial Measurement Unit (IMU) and the measurement of the performed distance (available through ABS wheels speed sensors). Many recent improvement in the characterization of acceleration and rotation rate measurement offsets due to thermal stability of microelectromechanical system components made these sensors compliant with car navigation requirements. However, random errors still remain. Consequences are as follows.

- Dead-reckoning drifts so much due to random errors integration, that detection and isolation of outliers in observations is not reliable (multipath affected observations remain statistically acceptable).
- Map-mismatching may happen, particularly inside dense urban centers, or at junctions.

Manuscript received July 01, 2008; revised April 15, 2009. Current version published October 21, 2009. This work was supported by the European project Cooperative Vehicle Infrastructure Systems (CVIS) by researchers of LCPC (Geo-localization Unit) and UTC (Heudyasic Lab), both partners of the Positioning and Mapping subproject POMA of CVIS, and the group of Intelligent Systems/University of Murcia, awarded as an excellence researching group in frames of the Spanish Plan de Ciencia y Tecnología de la Región de Murcia. The associate editor coordinating the review of this manuscript and approving it for publication was Dr. Dorota Brzezinska.

R. Toledo-Moreo, D. Bétaille, and F. Peyret are with the Laboratoire Central de Ponts et Chaussées, LCPC Nantes Centre, 44340 Bouguenais, France(e-mail: rafael.toledo@upct.es; david.betaille@lcpc.fr; francois.peyret@lcpc.fr).

J. Laneurit is with the Technical University of Compiegne, Compiegne 60205, France (e-mail: jean.laneurit@hds.utc.fr).

Color versions of one or more of the figures in this paper are available online at http://ieeexplore.ieee.org.

Digital Object Identifier 10.1109/JSTSP.2009.2027803

- Practically an acceptable maximum duration of GNSS outages constrains the availability of the application.

An alternative approach to 3-D IMU integration consists in approximating the problem in 2-D, assuming a planar movement of the vehicle. In this case, a single axis gyro only, coupled with the vehicle odometer, offers a good compromise. Once its position is determined, map-matching consists in vehicle tracking in map data with optimal criteria, like minimum distance point to segment, including heading difference vehicle to segment, etc., and taking advantage in this tracking process of connectivity between segments. A comprehensive summary of these techniques can be found in [3].

Whereas ego-localization and map-matching are made sequentially, Map Aided Localization will fuse the map data in the point positioning process itself altogether. Authors in [3] list these methods in a category called advanced map-matching algorithms.

Various research investigations were actually carried out by past on Map Aided Localization, among which are [4]–[10].

The way one can take into account the *a priori* information contained in road map vary from Bayesian filtering to fuzzy logic: in particle filters, suppression or down-weighting of particles far from the matched poly-line [7]; in extended Kalman filters, introduction of line heading or distance to line as a observation [9].

Our work claims a certain originality, to the extent that it combines a new description of road, including a detailed geometry, as well as a particle filter *a priori* suitable for multiple-hypothesis tracking in map data. To the authors' knowledge, none has used such a detailed description of the road geometry.

We actually make the assumption that the road network has been formerly surveyed. Reference [11] also presents a geometrical filtering of the trajectory, but in the Simultaneous Location And Mapping (SLAM) approach where the parameters of the road are identified in the same process as the ego-positioning itself. In order to increase the robustness of positioning, we will consider that the Emap is available *a priori*.

III. Overview of Emap Contents and Mapping Process

The objective of fusing GNSS, dead-reckoning, and Emap at lane-level accuracy requires first an offline mapping process, and second a real-time filtering system. The present section gives an overview of Emap contents as well as it summarizes the mapping process that was carried out for their construction. Real-time filtering will be addressed further in Section IV.

An Emap contains the geometrical description (by series of clothoids) of the middle of each lane of each carriageway. For us, a carriageway is a set of lanes having the same travel direction. It does not contain intersections, since we consider that large crossroads have not necessarily identified lanes in their middle, but only identified lanes until their bounds. Roundabouts, like crossroads, have not yet been modeled, but they should be in the near future (at least the larger ones, particularly those with several lanes). Exits and entrances of highways are completely represented, making locally an additional lane in the concerned carriageway. Clothoids are characterized by their origin coordinates, origin direction and curvature, and the variation rate of their curvature along with the curvilinear abscissas. Circles and straight lines are singular clothoids, either curvature or both curvature and its variation rate being null.

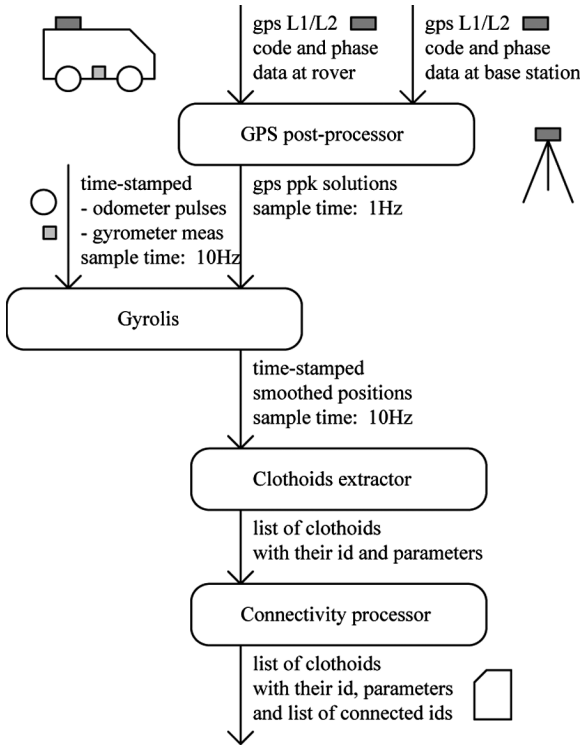

Fig. 1. Offline Emap data processing.

The computation of x, y Cartesian coordinates at a given abscissas consists in a couple of non-explicit integrals (known under the name of Fresnel integrals). With a computer, these integrals will be approximated by a classical piece-wise decomposition.

Differences between Emaps and standard maps delivered by map providers for car navigation systems today regarding the completeness and the accuracy of the geometry make the Emap model closer to ground truth than standard.

Fig. 1 shows the data flows included in the offline mapping process that we made [12]. The different steps of this process consist of the following.

1) Collecting GPS dual-frequency phase data, gyrometer, and odometer measurements on-board a vehicle used for mobile mapping the area.
2) Data postprocessing with a local GPS station, smoothing the kinematic solutions with the dead-reckoning sensors (this is made with our Gyrolis software [22]).
3) Extracting clothoids from the series of points.
4) Linking every clothoid to its neighbor to make topology available for further real-time map-matching.

A dedicated algorithm has been designed for computing the geometrical and topological features [12], with no implementation constraints since this process is executed offline. Each road element (each clothoid) is identified by its ID, and connected IDs are listed as attributes. They can be either at left or right, or in front of the current ID. Road elements are oriented similarly as the driving direction.

To conclude, let us notice that this mobile mapping and data processing were experimental, and they have not been optimized with the objective of an industrial production.

IV. GNSS/DR/Emap Data Fusion

This section focuses on the data fusion filter employed to integrate GPS positions corrected by EGNOS, dead-reckoning measurements, and the road shape data available in the Emap.

In the current literature, there are numerous filters applicable to nonlinear systems. Extended Kalman filters or EKF (linearizations of Kalman filter in different approximations), particle filters or PF (sequential Monte Carlo based methods), and unscented Kalman filter or UKF, (based on sigma-points) are some of the most employed in the researcher community. Each of them presents some benefits depending on the concrete implementation under consideration [6], [8], [13]–[19]

Among these methods, the particle filter is specially suitable for the issue addressed in this paper. As it will be shown, the functioning principle of particle filters results very convenient for the implementation of map observation updates.

A. Particle Filter Cycle

The principle of the particle filter is to represent by means of a set of N samples $\{X_k^i\}_{i=1}^N$ and their corresponding weights $\{w_k^i\}_{i=1}^N$ the probability density function $p(X_k/Y_{1:k})$ at instant k of the state vector $\mathbf{X}_k$, given past observations, is as follows:

$$p\left(\frac{\mathbf{X}_k}{Y_{1:k}}\right) \simeq \sum_{i=1}^{N} X_k^i \cdot w_k^i$$

where $Y_{1:k}$ stands for the observations collected from the initialization until instant k. Each sample X_k^i can be described as a Dirac delta expression $\delta_k^i(\mathbf{X}_k)$ in the form

$$\begin{aligned} \delta_k^i(\mathbf{X}_k) &= 0 \quad \text{if} \quad \mathbf{X}_k \neq X_k^i \\ \delta_k^i(\mathbf{X}_k) &= 1 \quad \text{if} \quad \mathbf{X}_k = X_k^i. \end{aligned} \tag{1}$$

The process of particle filtering can be summarized as follows.

1) Initialization: Generation of N particles, or samples of the state vector, X_0^i, with equal weights $1/N$.
2) Prediction: Estimation of X_{k+1}^i following the model dynamics.
3) Measurement update: Update of the weights of the particles with the observations Y_k, following the expression
$$w_k^i = w_{k-1}^i \cdot e^{\left(-0.5(Y_k - h(X_k^i))'(R^{-1})(Y_k - h(X_k^i))\right)}$$
where $h(X_k^i)$ is the observation function that relates at instant k the state X_k^i and observations Y_k (in our case it will be the second-order identity matrix), and R the covariance matrix of observations.
4) Normalization of the weights: $w_k^i = w_k^i / \sum_{i=1}^N w_k^i$.
5) Resampling: To prevent high concentration of probability mass on only a few particles, (leading to the convergence of a single w_k^i to 1), particles are resampled when next equation is verified
$$\frac{1}{\sum_{i=1}^{N} (w_k^i)^2} < 0.5N$$
6) End of cycle: Making $k = k + 1$, and iterating to step 2.

Further details of particle filtering can be found in [6].

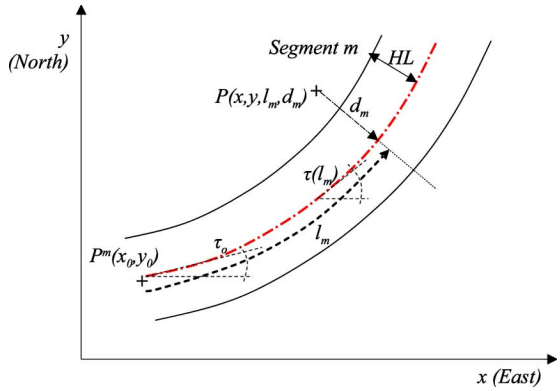

Fig. 2. Cartesian x, y and Frenet l^m, d^m coordinates for a point P, position of a vehicle driving segment m with a given half lane width HL. Initial angle of the segment τ_0, and angle at any Frenet abscissas $\tau(l_m)$.

B. Frenet/Cartesian Definition

The state vector of our filter is a composition of a Cartesian and a Frenet sub-states, $\mathbf{X} = [\mathbf{X}^C, \mathbf{X}^F]$, where $\mathbf{X}^C$ stands for the Cartesian part and $\mathbf{X}^F$ for the Frenet one (in the following, these superscripts will be used to distinguish both subsystems). $\mathbf{X}^C$ is defined by $[x, y, \psi]$, representing East, North, and heading angle, respectively, at the middle point of the rear wheel axle of the vehicle, while $\mathbf{X}^F$ includes $[l^m, d^m, m]$, that represent the values of abscissas and ordinates referred to the lane segment m. The state variables of the proposed filter are represented in Fig. 2.

The inclusion of Cartesian and Frenet definitions for the same point in the space introduces a partial redundancy in the state vector. However, the convenience of both sub-states in the filter state brings some benefits to the its implementation:

- On the one hand, Frenet variables are more adequate for evaluating the transitions between lane segments of the road. If the calculations required to carry out this process would have to be done by using Cartesian coordinates, the computational costs would constrain this solution only to applications in which the use of very high-end computers is feasible.
- On the other hand, the provision of East, North, and heading angle in a reference map appears necessary in a number of location based services in which this algorithm could be applied. In addition to that, the inclusion of a Cartesian sub-state allows uninterrupted navigation also when the Emap reference is not present. This is of special interest in very complex scenarios such as multiple lane crossroads where the definition of lane segments by means of clothoids becomes very difficult.

In spite of its benefits, the use of a partially redundant state vector implies some particularities in the implementation of the particle filter and its evolution model, that will be discussed along the paper.

1) Relation Between Frenet/Cartesian Reference Systems: Taking into account the proposed particle filter-based implementation, the notation of state vector for a particle i at instant k will be given by

$$X_k^i = [x_k^i,\ y_k^i,\ \psi_k^i,\ l_k^{m,i},\ d_k^{m,i},\ m_k^i]. \tag{2}$$

It is possible to relate both Frenet and Cartesian representations of the same point by means of the following expressions:

$$x = x_0^m + \int_0^{l^m} \cos(\tau^m(l^m))dl - d^m \sin(\tau^m(l^m))$$
$$y = y_0^m + \int_0^{l^m} \sin(\tau^m(l^m))dl + d^m \cos(\tau^m(l^m)) \quad (3)$$

where x_0^m, y_0^m are the East and North coordinates of the initial point of the road segment and $\tau_m(l^m)$ is the azimuth angle of the segment at abscissas l^m, given by

$$\tau^m(l^m) = \tau_0^m + \kappa_0^m \cdot l^m + \frac{c^m \cdot (l^m)^2}{2}. \quad (4)$$

being τ_0^m, κ_0^m and c^m shape parameters of the clothoid definition of segment m, and representing initial heading, initial curvature, and linear curvature rate, respectively. These are the parameters that define the clothoid description of the road shape (see Fig. 2).

C. Initialization of the Filter

The filtering process for the real-time navigation is schematically represented in Fig. 3. The basic idea is to explore multiple hypothesis for map matching using particles that move according to the vehicle dead-reckoning model. Update is either due to the Emap (applying a geometrical constraint that removes the particles beyond the bounds of their matched road element) or due to GPS observations. This process is explained in the next sections.

The filter begins with the initialization of the particles X_0^i. To realize this, first the Cartesian sub-state variables x, y are randomly generated following a Gaussian distribution with the first accepted GNSS point as mean value. Standard deviations values are proposed following the sensor specifications and the results obtained in our own trials described in Section V, being as follows:

- 0.3 m in case of using EGNOS;
- 0.1 m for the RTK receiver;
- 3 m for stand-alone GPS fixes.

Since it is assumed that no information about the initial heading is available, values of ψ^i are uniformly spread through the whole range of 2π radians.

For the initialization of the variables of the Frenet sub-state, $X_0^{F,i}$, we must first find out the lane segment in which each particle of the corresponding sub-Cartesian state $X_0^{C,i}$ is placed. With no *a priori* information of the vehicle position or orientation, it is not possible to employ topological or orientation information in the selection of the most appropriate road segment [3]. In this case, we assume that the computational time for the initialization is not necessarily bounded to real time constrains (this situation would happen only once and corresponds to the beginning of the circuit) and we follow a single-criterion method based on the distance to lane segments.

In the usual case that some *a priori* information about the vehicle positioning and its current road segment would be available for the initialization of the filter (for example, when the vehicle was previously navigating in the zone of an standard map and it enters in an area described by an Emap), this process could be assisted by that map, constraining the search to a very reduced number of Emap segments linked to the previous map arc, making possible a real time initialization process. Both possibilities, with and without *a priori* positioning and map information, are contemplated in the algorithm design. The problem of collaboration between commercial and our proposed enhanced maps is under study.

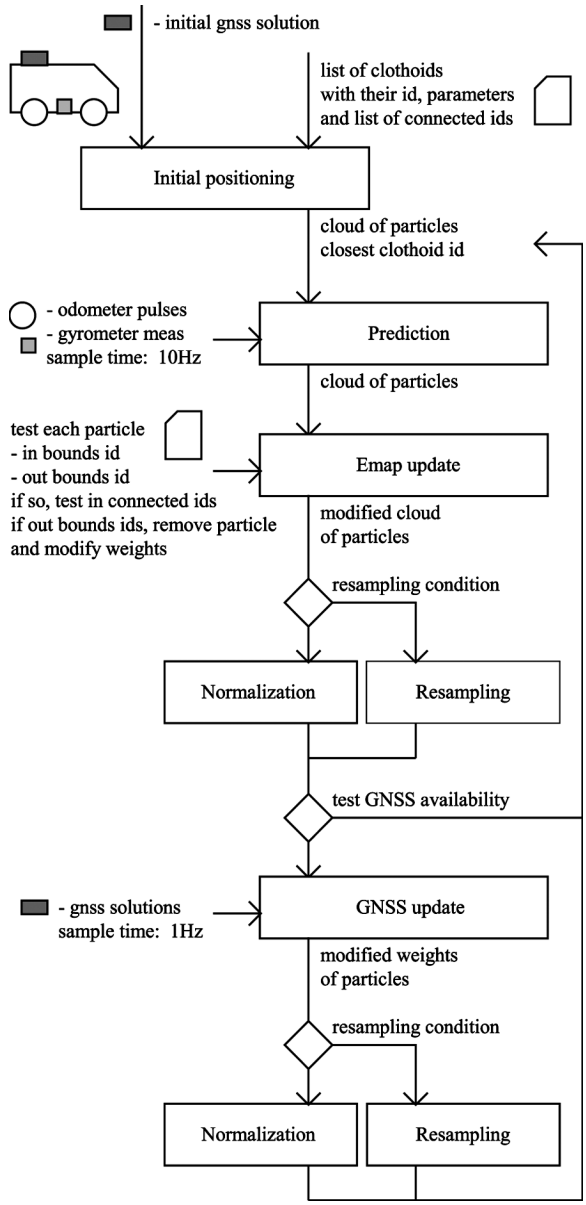

Fig. 3. Real-time GNSS/DR/Emap aided location.

Once the segment is chosen, Frenet variables referred to it $[l^{m,i},\ d^{m,i}]$ can be directly obtained since $d^{m,i}$ is the minimum distance between $[x^i,\ y^i]$ and segment $m(i)$, and $l^{m,i}$ its corresponding abscissas in the Frenet system (see Fig. 2). As can be noticed, $d^{m,i}$ is actually the value of the shortest distance found when searching the corresponding segment $m(i)$.

D. Filter Prediction

The prediction of the Cartesian sub-state for each particle will be calculated as follows:

$$x_{(k|k-1)}^i = x_{k-1}^i + \Delta_x^i$$
$$y_{(k|k-1)}^i = y_{k-1}^i + \Delta_y^i$$
$$\psi_{(k|k-1)}^i = \psi_{k-1}^i + \omega^i \quad (5)$$

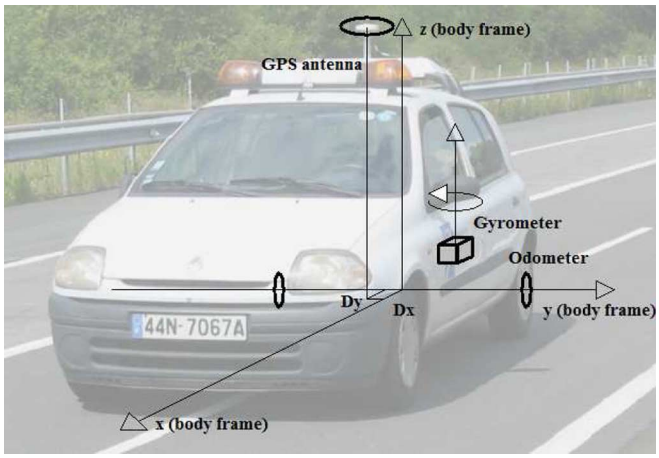

Fig. 4. Vehicle test prototype.

where

$$\Delta_x^i = ds^i \operatorname{sinc}\left(\frac{\omega^i}{2}\right)\cos\left(\psi^i + \frac{\omega^i}{2}\right) - \omega^i(Dx\ \sin(\psi^i) + Dy\ \cos(\psi^i)) + \delta_x^i \quad (6)$$

$$\Delta_y^i = ds^i \operatorname{sinc}\left(\frac{\omega^i}{2}\right)\sin\left(\psi^i + \frac{\omega^i}{2}\right) + \omega^i(Dx\ \cos(\psi^i) + Dy\ \sin(\psi^i)) + \delta_y^i \quad (7)$$

and

- ω^i is an input of the filter, and represents the vector of angular velocity values for every particle, following $\omega^i \sim N(\omega_{\text{gyr}}, \sigma^2_{\text{gyr}})$, where ω_{gyr} is the gyro measurement of the heading rate and σ_{gyr} its variance, that can be characterized using the angular random walk provided by its manufacturer.
- ds^i is an input of the filter, and represents the vector of traveled distance for every particle, that can be calculated by adding to the measurement of the traveled distance of the odometer, ds_{odo}, a uniform distribution of noise around $[-step_{\text{odo}}, step_{\text{odo}}]$, where $step_{\text{odo}}$ is the odometer step equal to 0.2615 m in our case.
- Dx and Dy are the Cartesian distances in the body frame of the vehicle between the position of the antenna and the middle point of the rear wheel axle, which is the assumed representative point for the vehicle pose (Fig. 4).
- terms δ_x^i, δ_y^i stand for the error in the prediction of $x^i_{(k|k-1)}, y^i_{(k|k-1)}$ in the navigation frame, modeled as random walk processes in such a way that after 1 s, the error due to the model inaccuracy is assumed to be 0.2 m, what was found a suitable tuning for our algorithm.

Fig. 4 illustrates the body reference frame and the positions of the sensors in our vehicle prototype.

As it can be noted, error terms that represent the distribution of particles were included in the prediction of the Cartesian substate. Hence, as each particle must refer to the same pose in both reference systems, the prediction of the Frenet variables will be dependent on the Cartesian estimates. By following this principle we manage that predictions errors are coupled in both reference systems.

Assuming straight movements between samples, it can be demonstrated that, for a given lane segment m, the prediction of the Frenet variables can be approximated by using the numerical expression

$$\begin{aligned} l^{m,i}_{(k|k-1)} &= l^{m,i}_{k-1} + cos(\tau^m)\Delta^i_x + sin(\tau^m)\Delta^i_y \\ d^{m,i}_{(k|k-1)} &= d^{m,i}_{k-1} + sin(\tau^m)\Delta^i_x - cos(\tau^m)\Delta^i_y \end{aligned} \quad (8)$$

that corresponds to a simple coordinate transformation (see Fig. 2).

E. Filter Update

Whether or not there are valid GNSS positions available at one execution step, the process of update will consist respectively of consecutive Emap and GNSS updates, or only the Emap update phase.

1) Emap Update: The prediction cycle presented in Section IV-D is applied at every input sample scan. However, as it was commented, the result obtained by (8) is only valid when the pose predicted for a particle i is still within the bounds of the segment associated to this particle at the instant that the prediction is made $(m_{(k|k-1)} = m_{(k-1)})$. Therefore, after every prediction phase the condition given by (9) must be verified by using the Emap observations

$$\left(0 < l^{m,i}_{(k|k-1)} < L^m\right) \quad \text{and} \quad \left(-\text{HL} < d^{m,i}_{(k|k-1)} < \text{HL}\right) \quad (9)$$

where L^m is the length of the segment in the Frenet abscissas (stored in the Emap) and HL is the value for the half of a lane width, assumed constant in our tests and with value 2.25 m. This value comes from the addition to 1.75 m (half of the width of a standard lane in Europe) of 0.5 m, that stands for an acceptable threshold of the error made in the mobile mapping process.

In case that (9) is satisfied, the prediction performed in (8) is accepted, and $m_k = m_{k-1}$. If any prediction of the Frenet variables does not verify (9), results of (8) must be disregarded and a different process must be followed. In this last case, two possibilities arise.

1) The vehicle moved from previous segment to a different one $m_k \neq m_{k-1}$ being new segment m_k in the list of candidates of m_{k-1} (stored in the Emap).
2) The vehicle is not within the bounds of any road segment and this particle must be eliminated, making $w^i_k = 0$.

To estimate the segment towards which the vehicle moved from m_{k-1}, a search based on distance criterion is launched among candidate segments. The reduced number of them (typically 3 or 4, and maximum 7 in the Emap of Cheviré bridge) keeps computational times of this search very low.

After the selection of the most likely segment, we must verify whether or not (9) is true. In case this expression is positive, we update the new value of m_k in the vector state and reevaluate $l^{m,i}_k, d^{m,i}_k$ according to it, in the same way that was performed in the last step of the initialization. In the negative case, this particle is eliminated by making its weight $w^i_k = 0$, and the weights must be normalized (step 3 of the particle filter cycle presented Section IV-A) for the rest of the active particles.

2) Resampling: We have seen that after every prediction, in the map update phase, the weights of those particles that do not verify the constraints given by map observations are set to zero.

Hence, to avoid a possible concentration of weights on only a few particles, the resampling condition introduced in step 4 of the algorithm (Section IV-A), must be evaluated. For computational reasons, in most of the cases this condition should be negative to prevent an excessive number of resamples. However, the condition must be effective to prevent a low number of active particles anytime.

Similar considerations regarding both Cartesian/Frenet subsystems as those made for the initialization must be taken into account. Following this idea, the Cartesian variables of the state are uniformly and randomly resampled, according to the cumulative distribution of the weights of the active particles, following a Kitagawa strategy for the redistribution [20]. For the estimation of the Frenet subsystem, in order to diminish the computational charges of the process, the number of candidate segments in which the new particle may lay must be constrained. In all the experiments carried out, it appeared that the corresponding new segments after every resample always belonged to the set of segments represented in the state variable m_k^i of the active particles. This implies typically only one or two possible segments associated to the new resampled Cartesian variables, and consequently a low computation. Finally, let us remind the need of estimating again new values for $l_k^{m,i}, d_k^{m,i}$ referred to the selected segment.

3) GNSS Update: When valid GNSS measurements are available, a GNSS update will be carried out just after the Emap update phase. Nevertheless, prior to the update with GNSS fixes, we must evaluate the quality of these data, in order to prevent from GNSS outliers (typically consequence of multipath effects). We decided to use the well-known Nyquist method based on the Mahalanobis distance. Details of how to implement it can be found in [21].

The GNSS update phase corresponds to step 2 of the particle filter cycle introduced in Section IV-A, and can be directly applied by simply making the following:

- $Y_k = [x_{GPS}, y_{GPS}]$, representing East and North values;
- $X_k^i = [x_k^i, y_k^i]$, that is, the Cartesian position subset of the state vector;
- function $h(X_k^i)$ will be the constant matrix H, described by $H = I_2$, the identity matrix of second order;
- $R = \sigma_{\mathrm{GNSS}} \cdot I_2$, where the value of σ_{GNSS} will depend on the GNSS position quality and was previously given in Section IV-C.

After the GNSS update, the normalization and the evaluation of the resample condition must be run again.

F. Navigation Out of the Emap Covered Area

Since Emaps are intended to cover specific areas of interest of the road network, a continuous definition of the road based on them should not be expected. For this reason, the algorithm must be prepared for interruptions in the provision of Emap observations. For example, due to the high complexity of the definition of lane segments in crossroads, in the current state of our investigations Emap data are not available when the vehicle enters these areas. In these situations, all the particles of the filter would be eliminated at the instant they leave the bounds of the last Emap segment (the case of the last selected segment being a segment with no neighbors). To prevent this, the algorithm was designed to be capable to navigate also in areas without Emap observations in a simple Cartesian mode. In this way, in those cases where no neighbors are found for the current set of m_k^i, the Frenet processes that involve Emap observations are disabled, and the vehicle navigates exclusively with the predictions of the Cartesian variables and the GNSS updates.

When running in Cartesian mode, at every prediction step the position of the vehicle is compared to the initial points of the Emap segments of the area of interest, and the distance from it to the closest segment is estimated. This calculation can be done very rapidly, since an Emap can only be joined through the initial points of its segments. In case that, the distance value is lower that 2.25 m (assumed width of half a lane), the algorithm switches to Frenet/Cartesian mode and keeps working with all its functionalities.

V. Experimental Tests

Main objectives of the experiments presented in this section are as follows.

1) Validation of the proposed map model based on sets of interconnected clothoids to describe precisely the horizontal alignment of the road at lane level.
2) Analysis of the EGNOS capabilities as the plausible GNSS data source for lane-level-based services, taking into account aspects such as its accuracy, coverage, and integrity.
3) Evaluation of the proposed GNSS/DR/Emap data fusion filter with real data-sets in a complex scenario with multiple lane roads.
4) Determination of the capabilities of the particle filter as the data fusion technique for fusing GNSS/DR/Emap, taking into account computational aspects.
5) A comparison between integrated GNSS/DR and GNSS/DR/Emap based solutions to the problem of lane-level positioning of a road vehicle.

For these purposes, different campaigns were carried out in the area of Nantes, France, near the facilities of the LCPC Center. Prior to the presentation of the test results, the prototype employed in our experiments is briefly introduced.

A. Test Vehicle Prototype

Fig. 4 shows the test vehicle used for collecting data-sets and evaluation purposes. The vehicle was equipped with the following sensors.

- EGNOS capable GPS receiver: Trimble Ag 132, mono-frequency, L1.
- Dual-frequency RTK receiver for evaluation: ZMax by Ashtech.[1]
- Yaw rate gyroscope: E-core RD-2000 FOG gyro by KVH.
- One odometer with resolution of 1 pulse per 26.15 cm placed on the gear box coupled to the rear wheels axle.

For this research, we are using a fiber-optic gyrometer (FOG), despite its cost does not comply with automotive requirements. This sensor deployment serves well our purposes of validating the algorithm under proposition. Nevertheless, the cost of on-board unit could be optimized with hardware such as near tactical grade MEMS, which would certainly apply. Additional tests should be done for showing comparative results of different instrumentation.

[1]The RTK Zmax by Ashtech was also used for the elaboration of the Emap.

Fig. 5. Mappy (TeleAtlas data) map rendering of Cheviré south interchange. One-way roads are represented by one poly-line, which makes two poly-lines for highways (in blue), and one for exits (in orange). Shape points are visible in curves. Multiple lane exits are simplified. Lanes separation due to bridge piles at highways crossing is not represented.

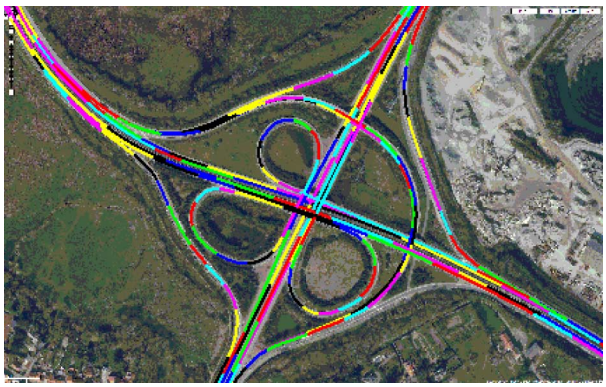

Fig. 6. Emap made by mobile mapping superimposed onto a Google Earth image. Each color represent a different clothoid.

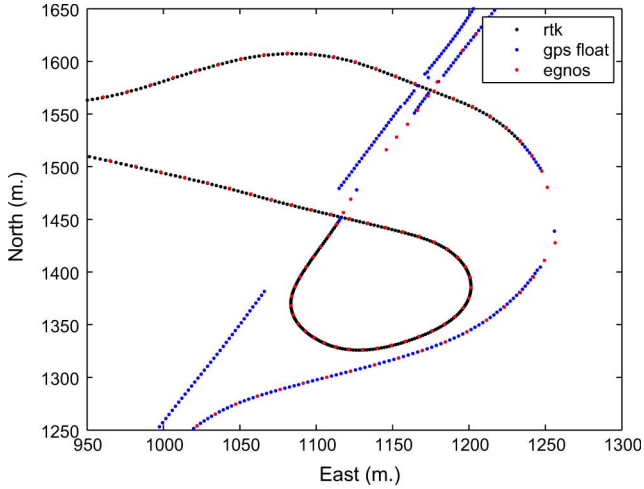

Fig. 7. RTK fix (dotted black), RTK float (dotted blue) and GPS/EGNOS (dotted red) values logged in this test scenario.

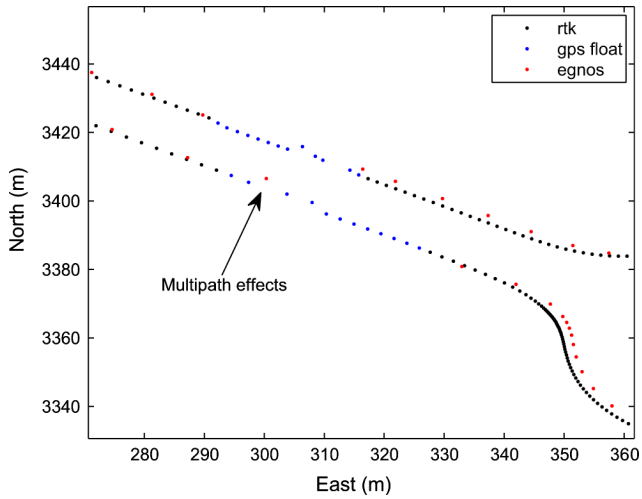

Fig. 8. Availability and multipath problems of GPS/EGNOS (dotted red), RTK fix (dotted black) and RTK float (dotted blue) in a road stretch of the test.

B. Validation of a Piece-Wise Clothoid Based Map Model

Fig. 5 displays a standard map rendering of the Cheviré south interchange, whereas Fig. 6 superimposes a Google image and the mobile mapping output. Each color represents a different clothoid, extracted from postprocessed kinematic (PPK) GPS solutions, smoothed using odometry and yaw rate measurement [12], [22]. The estimated accuracy has an order of magnitude of a few decimeters (this accuracy can reasonably be bounded by 0.5 m), mainly due to the unknown exact lateral position of the vehicle in its lane, when surveying. This 0.5 m is considered as compatible with the Emap-based CVIS applications. In case of future higher accurate requirement, additional vision on-board could help improving this accuracy.

C. Exploitation of EGNOS

Benefits that EGNOS should bring to the proposed navigation system are as follows:

- augmentation of the positioning accuracy, thanks to the GPS corrections broadcast by the geostationary satellite;
- provision of positioning integrity, by means of the integrity values included in EGNOS, that allow the calculation of the SBAS-based horizontal protection level (HPL) and vertical protection level (VPL) parameters.

In this section, we focus exclusively on accuracy aspects, since the study of the integrity aspects requires a very specific and detailed attention.

For evaluation purposes, RTK and GPS/EGNOS positions were logged simultaneously during the same trajectory along the Cheviré bridge Emap. Fig. 7 shows a stretch of the resultant positions. As it can be seen, the availability of satellite signals is affected in a similar manner in both GPS/EGNOS and GPS solutions. In this image, we have distinguished between RTK fixed values (in dotted black) and RTK float values (dotted blue), *a priori* less precise. The need of extra sensors not only for navigation purposes, but also for the elaboration of the Emap, is clear from this image.

Apart from the gaps of coverage, some other problems were found during the tests performed. Fig. 8 shows the effects of multipath propagation of the satellite signal. As can be easily seen, the multipath phenomenon affects both EGNOS-aided GPS (red dotted) and dual frequency RTK GPS (blue dotted) in this part of the trajectory. This confirms that EGNOS corrections cannot solve the multipath problems of GPS, one of its

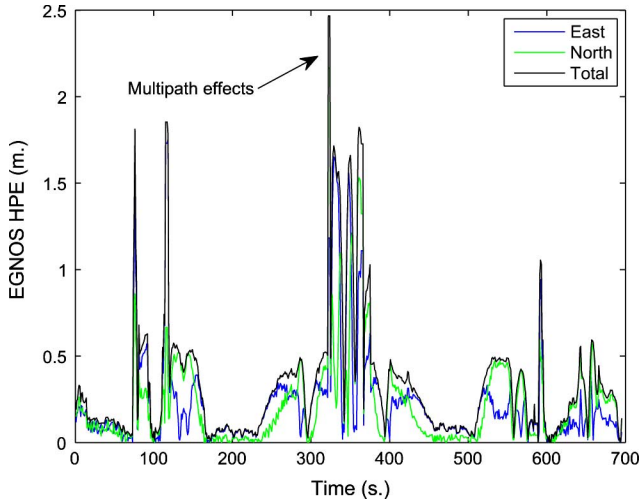

Fig. 9. Estimates of the horizontal positioning error (HPE) for East (solid blue), North (solid green) coordinates and total horizontal error (solid black) obtained by GPS/EGNOS in this test scenario.

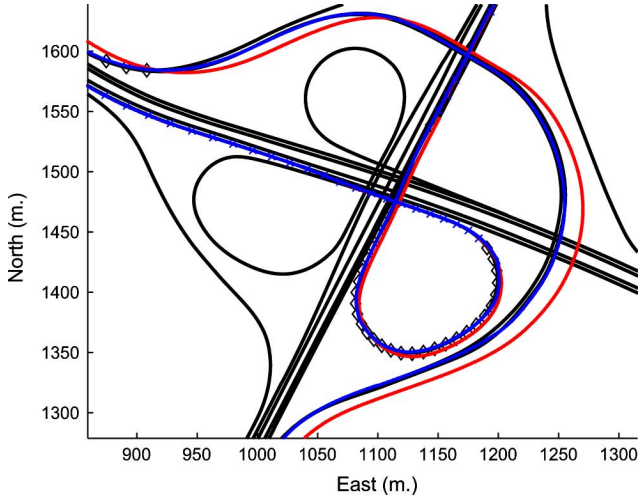

Fig. 10. Stretch of the trajectories provided by the FCPF (solid red) and the SCPF (solid blue), referred to the Emap (solid black). EGNOS positions (black diamonds: ⋄) were masked during periods of 110 and 30 s.

most problematic issues since consequent errors are not properly considered by integrity figures that reflect signal-in-space errors.

The estimated horizontal positioning errors (HPE) accomplished by EGNOS-corrected GPS along the whole trajectory test can be seen in Fig. 9. For the estimation of this error, RTK values are assumed to provide the true path. GPS/EGNOS values were collected at the frequency rate of 1 Hz, being the total test duration higher than 11 min. As it is confirmed in this image, multipath propagations impoverish noticeably the quality of the solution. The mean value of the horizontal position error during this test was 0.345 m, with standard deviation of 0.382 m, values that encourage the use of EGNOS in our system. However, a maximum error of 2.467 m is still too far from the aimed performance of the GNSS sensor aboard. To overcome this problem, we are currently conducting investigations on the detection of outliers in GPS/EGNOS positions.

D. Evaluation of the Proposed GNSS/DR/Emap Fusion

1) Positioning Accuracy: This section discusses the accuracy of the proposed GNSS/DR/Emap fusion algorithm (being GNSS an EGNOS-capable GPS in our case). To do it so, our proposal was compared to some other state-of-the-art fusion techniques. The results presented next show the benefits achieved in terms of accuracy as compared to a GNSS/DR solution running a particle filter. Some other tests with GNSS/DR based EKF solutions were realized obtaining similar results to the GNSS/DR based PF. However, the PF approach was found less dependent of good initial conditions, what it consistent with the literature of the topic [23], [24]. For this reason, and taking into account that the computational demand of the PF verified the realtime constraints, this was finally selected for the comparison. In the following, the GNSS/DR/Emap PF is noted as Frenet Cartesian Particle Filter (FCPF) and the GNSS/DR PF is noted as Single Cartesian Particle Filter (SCPF).

Let us remark here that to the authors' understanding, a comparison between a navigation solution and a map-matching solution would bring no conclusions in terms of accuracy, and for this reason it has not been performed. As it is traditionally understood in the literature, map-matching processes provide positions projected on a map segment (typically its centerline). The concept of map-matching is associated to the determination of the road segment any time, and consequently the final position accuracy is determined by the accuracy of the map itself. By contrast, our algorithm does not project the position of the vehicle to the map segments or centerlines. Each particle of our filter can freely move according to the filter inputs and the vehicle model within the limits of the segment to which it is associated. Therefore, the accuracy of the results is not exclusively determined by the map, although map observations affect its value as long as they constrain the position of each particle to the map segment bounds. The determination of the vehicle position anywhere within the edges of the carriageway can be found an important contribution to map-matching for transport applications [3].

A stretch of the trajectories achieved by both the SCPF and the FCPF during a test with a GPS mask of 110 s is displayed in Fig. 10. In this image, solid black line represents the Emap, blue the SCPF solution, red the FC, and EGNOS positions are represented by black diamonds (⋄). SCPF presents good results, with low drifts as compared to some methods proposed in the literature. Nevertheless, in cases of long GNSS outages, it is a matter of time that the estimated position drifts, due to the accumulation of errors in the dead-reckoning sensors and the vehicle model.

On the other hand, the proposed FCPF presents no drifts along the same stretch of the road, obtaining similar results during every trial. The use of Emap observations that take into account the road geometry maintains the particles within the bounds of Emap segments. The result is that particles are adapted at every filter execution step to the Emap segments shape, and drifts are constrained to the segments limits.

Fig. 11 shows the positioning errors accumulated by both SCPF and FCPF methods during a test performed following the same trajectory employed for the test presented in Fig. 10. True reference at every instant is assumed to be given by RTK

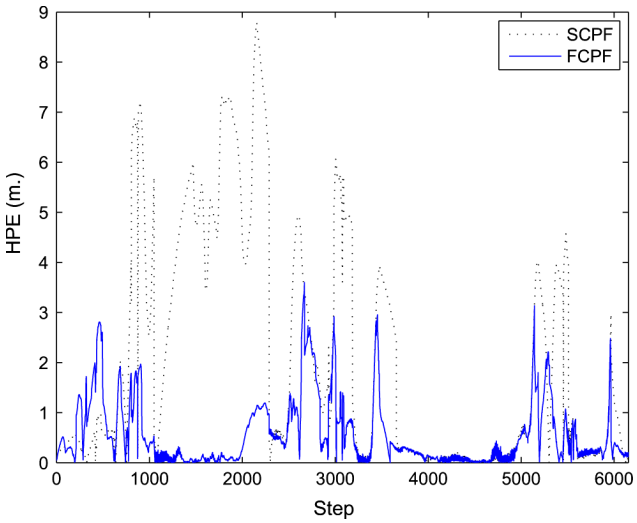

Fig. 11. Horizontal positioning errors (HPEs) obtained by both SCPF and FCPF algorithms in a test through Cheviré bridge.

TABLE I
SOME STATISTICAL VALUES ACHIEVED BY SCPF AND FCPF DURING A TEST ALONG THE EMAP

Filter	Mean	Std	Max
SCPF	2.13	2.35	8.79
FCPF	0.57	0.67	3.56

fixes and two periods of EGNOS masks of 110 and 30 s duration were simulated to test the performance of the system under poor coverage conditions. In the analysis of accuracy values, periods without RTK fixes were not considered for the evaluation, to avoid possible mistakes derived from interpolation processes. In addition to that, the stretches outside the Emap covered area were also removed for the same reason.

Table I summarizes some statistical values of interest obtained in this test. These results appeared consistently during all the trials performed, and yield several conclusions.

1) The results achieved by the SCPF are good as compared to the values obtained by similar systems reported in the literature.
2) Nevertheless, a mean value of 2.13 m with standard deviation of 2.35 m is not good enough for lane-level location-based applications.
3) The inclusion of Emap observations in a combined fusion/matching process increases the accuracy of the provided positioning.
4) The values achieved by the proposed FCSP of 0.57 m and 0.67 m for mean and standard deviation, respectively, are good enough for lane-level matching and positioning. If a Normal distribution is assumed for the HPE values, the proposed FCPF filter provides more than the 95% of the output positions within an error ellipsis of 1.9 m, even in cases with very long absences of GNSS positions (110 s).
5) The maximum value of 3.6 m corresponds, as a matter of fact, to a stretch with EGNOS coverage, in which an EGNOS outlier due to multipath effects was not properly classified by the Nyquist test. Therefore, the effective elimination of multipath effects in EGNOS positions appears to be very recommendable for the application of lane-level based safety and comfort applications.

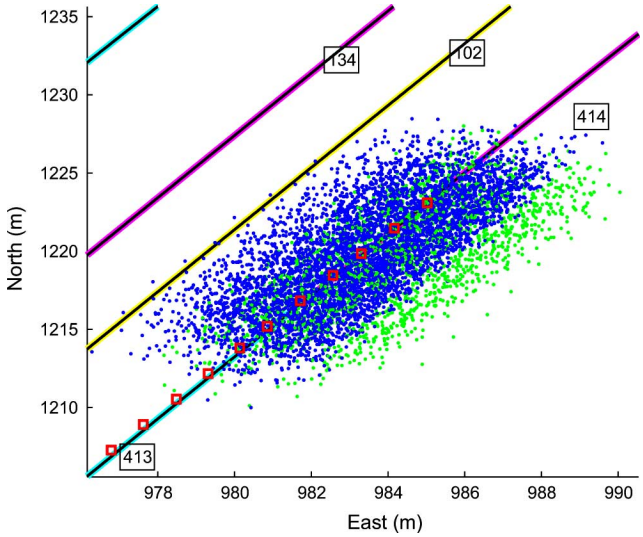

Fig. 12. Example of particles dispersion in parallel lane segments. Lane segments are represented in cyan, violet, and yellow solid lines with a thinner black solid line in the middle and identifiers within a bounding box in the middle value of their abscissas. Green points correspond to the positions of the predicted particles during a few filter steps. Blue points are the remaining particles after the Emap update phase. Finally, red squares stand for the filter positioning output.

2) Lane Occupancy: Fig. 12 shows an example of particle propagation and the result of updating with the Emap observations. Road segments are represented in cyan, violet, and yellow colors with a longitudinal black solid line and the identifiers within a bounding box in the middle value of their abscissas. The dispersion of the predicted positions for the particles (green points) depends on the error assumed for the inputs and the prediction model, becoming higher with high error considerations. Blue points represent particles with non-null weight (survivors after the Emap update). It can be clearly seen where is the bound for the right side of the lower lanes with labels 413 and 414 (consecutively in cyan and violet). However, on their left side some particles appear "alive" although they are much further than the 2.25 m value for half a lane. This is due to the fact that these particles are assigned to segment 102, and placed within its bounds. In the same figure, red squares represent the weighted composite positioning solution provided by the filter. The elimination of those particles that laid outside the limits of the segment avoided the filter solution to drift out of the road (the accumulation of green points is clearly offset to the right). Although some particles were assigned to segment 102, due to its limited number and weight their influence on the filter output is almost negligible.

The probability that the vehicle occupies lane segment r at instant k $\mu^{m=r}$ can be easily calculated as the addition of the normalized weights of those particles that are associated to segment r as follows:

$$\mu_k^{m=r} = \sum_{i=1}^{N} w_k^{i|m=r}. \tag{10}$$

The provision of probability values for lane segment occupancy anytime offers a first solution to the problem of map-matching at lane level, answering the question "in which lane the vehicle is," and brings another important contribution to map-matching for transport applications [3].

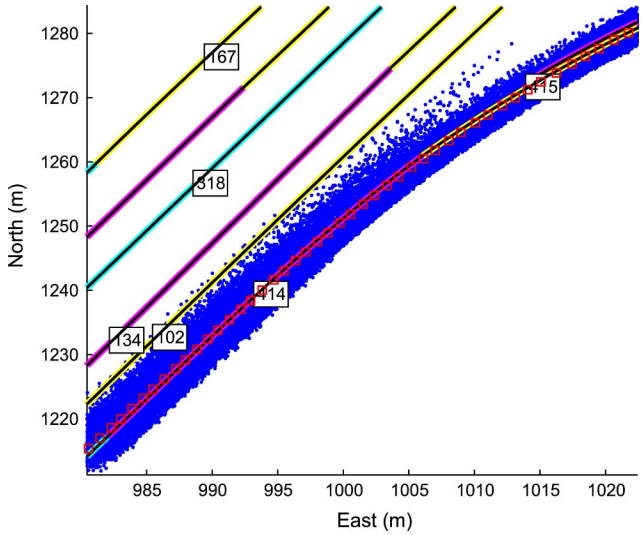

Fig. 13. Particles dispersion and filter solution in the case of the vehicle taking a highway exit. Lane segments are represented in cyan, violet, and yellow solid lines with a thinner black solid line in the middle and identifiers within a bounding box in the middle value of their abscissas. Blue points stand for the particles with non-null weight after the Emap update phase. Red squares represent the filter positioning output.

3) Multi-Hypothesis Capabilities: Fig. 13 presents one very common situation on highway environments that typically induces errors in map matching algorithms. As it was commented, lane segments are represented as solid cyan, violet, and yellow lines with a black thinner line and their identifiers. For the sake of clarity in the image, on this occasion predicted positions for each particle have been omitted and only active particles after the Emap updates are plotted. GNSS values were masked during this test and therefore are not included in the graph.

The capability of the proposed particle filter for multi-hypothesis tracking can be observed in this image. The main core of the particles are distributed around segments 414 and 415. Predicted particles out of their bounds were removed from the solution by making its weight equal to zero. The filter positioning output represents therefore a vehicle driving from segment 414 to segment 415, what corresponds to the real trajectory of the vehicle. However, some particles that laid out of the limits of segments 414 and 415 were not removed, and their predictions were considered valid during some filter steps. It is the case of the particles of the upper side of the image that were associated to segment 102. These were kept "alive" until their predictions were located outside of this segment bounds. Despite the fact that these particles represent a very small part of the whole set and their influence on the solution is almost negligible, the possibility of having different sets of particles associated to multiple lanes bring some very positive benefits to our algorithm: in the process of map-matching for the determination of the vehicle trajectory there is no need to make a "fast" decision about the lane segment in which the vehicle is. On the contrary, it is possible to benefit from multiple threads of probability values for several lanes, making possible a "slow" decision as the particles evolve at every filter step (what depends on the vehicle model and the inputs anytime). This can be found very useful to prevent from many errors in segment assignments that lead to corrupted map-matched solutions and the necessary re-initialization of the positioning system [3].

TABLE II
PROBABILITIES OF LANE OCCUPANCY DURING A SHORT STRETCH OF THE TEST

Step	μ^{414}	μ^{415}	μ^{102}
$k-3$	0.91	0.00	0.09
$k-2$	0.59	0.35	0.06
$k-1$	0.21	0.76	0.03
k	0.00	0.99	0.01

TABLE III
COMPUTATION TIMES OBTAINED WITH DIFFERENT NUMBERS OF PARTICLES

Test duration	Number of particles	Computational time
674 s	500	178 s
	1000	354 s
	2000	668 s

Table II shows the probability values calculated following (10) and associated to each lane at several instants of the stretch shown in Fig. 13. As the particles associated to segment 102 evolve and leave the segment, the probability that the vehicle occupies lane segment 102 diminishes. We can also appreciate the transition from segment 414 to 415.

As a consequence of the multi-hypothesis feature of the algorithm and the diminution of the probability values of one segment, the number of particles decreases. Let us remind here that, following the PF principles presented in Section IV-A, particles must be resampled to avoid the deterioration of the solution.

4) Computational Aspects: Since the algorithm must be capable to provide real-time positioning to a road vehicle, computational aspects were taken into account in its implementation. Different experiments were realized with different number of particles and circuits. Table III shows the computational times obtained with different number of particles during the test on Cheviré bridge, running in Matlab and using a standard laptop at 1.67 GHz. The results obtained with both 500 and 1000 particles were very good. Nevertheless, 1000 was found more robust in some cases of particularly bad conditions, such as simulated GPS masks of long duration. The results presented in this section were obtained with 1000 particles. As can be seen in this table, these results show the capability of the algorithm to be executed under real-time conditions. Even so, due to the importance of this issue future work will be focused on the computational aspects of the algorithm and its implementation on a single-board computer.

VI. CONCLUSION AND FUTURE WORK

This paper presented a novel algorithm for the localization of vehicles at the lane level, employing EGNOS-capable GPS, dead-reckoning, and map observations. In addition to that, a new method to define road lane segments as a piece-wise set of clothoids for the horizontal alignment was proposed. These proposals were evaluated in real complex scenarios with multiple lanes. Main contributions achieved in these investigations are as follows.

- An Emap (enhanced map) based on a geometrical representation of each road lane with series of clothoids was proposed. This Emap can supply to vehicular applications information of the road geometry and topology at the lane level, and can be very useful for many systems such as navigation, lane determination, or lane departure warning systems.

- The inclusion of the observations of the Emap in the algorithm for vehicle navigation brings important benefits in terms of accuracy. The navigation filter proposed in this paper was compared to a state-of-the-art solution such as a GPS/EGNOS/DR running a particle filter, obtaining much better results in usual situations of poor satellite coverage.
- The vehicle positions provided by the filter can be anywhere within the edges of the carriageway (contrary to the traditional map-matched positions projected in the centerline of the map segment). Each particle of our filter can freely move according to the filter inputs and the vehicle model within the limits of the segment to which it is associated.
- The provision of probability values for lane segment occupancy anytime offers a solution to the problem of "in which lane the vehicle is." To the best of the authors' knowledge, the problem of lane occupancy was not solved yet in the literature.

Additionally, the capability of GPS/EGNOS to be employed as GNSS data source for our purposes was also studied. Results show that although accuracy values in normal operation are good enough to meet the demanded standards, outliers as a consequence of multipath effects impoverish noticeably the performance quality of the system. An efficient method to detect and remove these outliers must be found before being capable to completely rely on GPS/EGNOS to this problem.

Finally, some other future works will be focused on the use of 3-D Emaps and a 3-D positioning filter, with terrain modeling and tightly coupled GNSS data.

REFERENCES

[1] F. Peyret, D. Bétaille, J. Laneurit, and R. Toledo-Moreo, "Lane-level positioning for cooperative systems using EGNOS and enhanced digital maps," in *Proc. ENC GNSS Congr.*, Toulouse, France, 2008, paper 0105.

[2] J. Chao, Y. qi Chen, W. Chen, Z. Ding, N. Wong, and M. Yu, "An experimental investigation into the performance of GPS-based vehicle positioning in very dense urban areas," *J. Geospatial Eng.*, vol. 3, pp. 59–66, 2001.

[3] M. A. Quddus, W. Y. Ochien, and R. B. Noland, *Current Map-Matching Algorithms for Transport Applications: State-of-the-Art and Future Research Directions*. New York: Elsevier Transportation Research Part C, vol. 15, pp. 312–328.

[4] E. J. Krakiwsky, C. B. Harris, and R. V. C. Wong, "A Kalman filter for integrating dead-reckoning, map-matching and GPS positioning," in *Proc. IEEE Pos. Loc. Nav. Symp.*, Orlando, FL, 1988, pp. 39–46.

[5] C. A. Scott, "Improved GPS position for motor vehicles through map-matching," in *Proc. ION GPS Conf.*, Salt Lake City, UT, 1994, paper 37.

[6] F. Gustafsson, F. Gunnarsson, N. Bergman, U. Forssell, J. Jansson, R. Karlsson, and P. J. Nordlund, "Particle filters for positioning, navigation, and tracking," *IEEE Trans. Signal Process.*, vol. 50, no. 2, pp. 425–437, Feb. 2002.

[7] K. W. Lee, S. Wijesoma, and J. I. Guzman, "A constrained SLAM approach to robust and accurate localization of autonomous ground vehicles," *Robot. Autom. Syst.*, vol. 55, pp. 527–540, 2007.

[8] A. N. Cui, L. Hong, and J. R. Layne, "A comparison of nonlinear filtering approaches with an application to ground target tracking," *Signal Process.*, vol. 85, no. 8, pp. 1469–1492, 2005.

[9] C. Fouque, Ph. Bonnifait, and D. Bétaille, "Enhancement of global vehicle localization using navigable road maps and dead-reckoning," in *Proc. IEEE Pos. Loc. Nav. Syst. Symp.*, Monterey, CA, 2008, pp. 1286–1291.

[10] M. A. Quddus, R. B. Noland, and W. Y. Ochieng, "A high accuracy fuzzy logic-based map-matching algorithm for road transport," *J. Intell. Transportation Syst.: Technol., Plan., Operat.*, vol. 10, no. 3, pp. 103–115, 2006.

[11] Y. Cui and S. S. Ge, "Autonomous vehicle positioning with GPS in urban canyon environments," *IEEE Trans. Robotics and Automation*, vol. 19, 2003.

[12] D. Betaille, R. Toledo-Moreo, and J. Laneurit, "Making an enhanced map for lane location based services," in *Proc. IEEE ITSC'08*, 2008, pp. 711–716.

[13] R. Toledo, M. Zamora, B. Ubeda, and A. Skarmeta, "High-integrity IMM-EKF-based road vehicle navigation with low-cost GPS/SBAS/INS," *IEEE Trans. Intell. Transport. Syst.*, vol. 8, no. 3, pp. 491–511, Sep. 2007.

[14] N. Yang, W. Tian, Z. Jin, and C. Zhang, "Particle filter for sensor fusion in a land vehicle navigation system," *Meas. Sci. Technol.*, vol. 16, pp. 677–681, 2005.

[15] E. Shin and N. El-Sheimy, "Unscented Kalman filter and attitude errors of low-cost inertial navigation systems," *Navigation, J. Inst. Nav.*, vol. 54, p. 1.9, 2007.

[16] R. Merwe, E. Wan, and S. Julier, "Sigma-point Kalman filters for nonlinear estimation and sensor-fusion: Applications to integrated navigation," in *Proc. AIAA Guid., Nav., Contr. Conf. Exhibit*, Rhode Island, 2004 [Online]. Available: http://choosh.csee.ogi.edu/spkf/spkf_files/vanderMerwe_GNC2004.pdf

[17] M. St-Pierre and D. Gingras, "Comparison between the unscented Kalman filter and the extended Kalman filter for the position estimation module of an integrated navigation information system," in *Proc. IEEE Intell. Veh. Symp.*, Parma, Italy, Jun. 2004, pp. 831–835.

[18] J. J. Laviola, "A comparison of unscented and extended Kalman filtering for estimating quaternion motion," in *Proc. Amer. Control Conf.*, 2003, pp. 2435–2440.

[19] S. Julier and J. K. Uhlmann, "Data fusion in nonlinear systems," in *Handbook of Multisensor Data Fusion*, D. Hall and J. Llinas, Eds. Boca Raton, FL: CRC, 2001.

[20] F. Campillo, *Filtrage Particulaire and Modèles de Markov Cachés,* 2006 [Online]. Available: http://ftp.irisa.fr/local/sigma2/campillo/cours/2006-master2-toulon.pdf

[21] Y. Bar-Shalom and X. R. Li, *Estimation and Tracking: Principles, Techniques and Software*. Norwood, MA: Artech House, YBS Publishing, 1998.

[22] D. Bétaille, "GYROLIS: Logiciel de localisation de véhicule en post-traitement par couplage GPS—gyromètre—odomètre," *Bull. Spécial Instrum. des Laboratoires de Ponts et Chaussées*, no. 275, pp. 75–87, 2008.

[23] A. Dumitrache, M. A. Zamora, R. Toledo-Moreo, and A. G. Skarmeta, "Hybridized GPS/DR positioning system with unknown initial heading for land vehicles," in *Proc. IEEE ITSC'08*, Beijing, China, 2008, pp. 974–979.

[24] M. A. Zamora, D. Bétaille, F. Peyret, and C. Joly, "Comparative study of extended Kalman filter, linearised Kalman filter and particle filter applied to low-cost GPS-based hybrid positioning system for land vehicles," *Int. J. Intell. Inf. Database Syst.*, vol. 2, no. 2, pp. 149–166, 2008.

Rafael Toledo-Moreo (M'08) received the M.S. degree in automation and electronics engineering from the Technical University of Cartagena (UPCT), Cartagena, Spain, in 2002 and the Ph.D. degree in computer science from the University of Murcia (UMU), Murcia, Spain, in 2006.

He is an Assistant Professor with the UPCT, Research Member of the group of Intelligent Systems with the UMU, member of the IFAC Technical Committee on Transportation Systems, the IEEE-RAS TC for Intelligent Transportation Systems, associate editor and IPC, member of several conferences (IEEE-ITSC, IEEE-IV, IEEE-IROS, IEEE-ICVES, IFAC-CTS) and guest editor of one journal (IJIIDS). His main field of interest is road navigation systems.

David Bétaille (M'09) received the Ph.D. degree from University College London, London, U.K., in 2004, for his investigations on phase multipath in kinematic GPS.

He is a Researcher in the Geolocalization research team at the Laboratoire Central de Ponts et Chaussées (LCPC), Bouguenais, France, where his current activities relate to vehicles positioning by satellites systems combined with dead-reckoning and mapping. ADAS and in general road safety applications compose the research context of his lab.

François Peyret received the M.S. degree in mechanical engineering from ENSMA, Poitiers, France in 1974.

He is currently Director of Research (equivalent of Professor), and head of the Image Processing and Geopositioning Research Team, atLaboratoire Central de Ponts et Chaussées (LCPC), Bouguenais, France, where he is leading research activities in the field of road vehicle positioning for ADAS, especially with hybrid GNSS systems and enhanced 3-D map-matching. His team is currently involved in two major European integrated projects in this field: CVIS and SAFESPOT from the 3-D eSafety call and also in several national projects or research actions.

Jean Laneurit received the Ph.D. degree from the University Blaise Pascal, Clermont, France, in 2006.

His research interests include data processing and data fusion. During his postdoctoral fellowship, he worked on navigation systems and especially on map matching using particle filtering. In September 2008, he joined the French National Institute for Research In Computer Science and Control. Currently, his research is focused on computer vision and augmented reality.